

Linear Solvation Energy Parameters for Model Tropospheric Aerosol Surfaces

Ephraim Woods, III,* Carl N. Wivagg, and Daniel Chung

Department of Chemistry, Colgate University, 13 Oak Drive, Hamilton, New York 13346

Received: December 22, 2006; In Final Form: February 23, 2007

Excited-state absorption spectra for several coumarin derivatives adsorbed to aerosol particles provide linear solvation energy (LSE) relationships for the aerosol surfaces. This study focuses on NaCl and $(\text{NH}_4)_2\text{SO}_4$ particles as models for tropospheric aerosol. We investigate several others, including NH_4Cl , NaBr, KI, Na_2SO_4 , NaNO_3 , Al_2O_3 , and CaCO_3 , to establish trends and understand the factors that control polarity for surfaces. The Kamlet-Taft dipolarity/polarizability parameter, π^* , for these particles ranges from 0.73 to 1.69. The values are high compared to most homogeneous molecular solvents and are attributable to ion–dipole forces, especially at defect sites. We also find that the smaller values of π^* (1.01 for $(\text{NH}_4)_2\text{SO}_4$ and 0.73 for NH_4Cl) correlate with appreciable hydrogen bond donor acidity in the surface ($\alpha = 0.23$ and 1.06, respectively). Strong hydrogen bonds with the surface lead to a drop in overall polarity either by making interaction with very polar defect sites less likely or orienting the probe molecule away from the surface. Adsorbed water layers mainly alter the α value of the surface, but can have indirect effects on π^* by changing the interaction of the adsorbed molecule with the surface.

I. Introduction

Aerosol particles play several important roles in the atmosphere. They alter Earth's climate through the scattering and absorption of radiation, contribute to cloud nucleation, and serve as reactants in, or hosts to, a wide range of chemical reactions. Each of these roles depends directly on the electronic properties of the particles' surfaces. Light scattering depends on the refractive index and cloud nucleation on the interaction potential of the surface with gaseous water. Certainly, the extent to which a particle surface can mediate or participate in chemical reactions is a function of the electronic structure of the atoms near the surface. A clear, quantitative description of these properties is important, then, in developing a clear picture of particle processes in the atmosphere.

In the context of chemical reactivity, chemists often use the idea of polarity to describe the important electronic characteristics of a chemical environment, and these typically include dipolarity and polarizability as well as hydrogen bond acidity or basicity. The concept of polarity is usually applied to molecular, homogeneous solvents. In fact, several empirical scales have been developed to quantify polarity for these solvents.¹ Many polarity scales involve measuring the electronic spectroscopy of a polarity indicator molecule whose energy levels are highly solvatochromic, or particularly sensitive to the chemical environment. For example, the $E_T(30)$ scale is a single-parameter measure of polarity that is equal to the energy in kcal/mol of the lowest $\pi-\pi^*$ transition in a pyridinium N-phenolate betaine dye.¹ This single-parameter approach is powerful and widely applicable, but is limited in its ability to describe strongly hydrogen-bonded systems.² Another approach, introduced by Kamlet, Abboud, and Taft,^{3–5} quantifies dipolarity and polarizability separately from hydrogen-bonding character using a multi-parameter approach. Our goal is to adopt this multi-parameter approach in the characterization of aerosol particle surfaces that are important in tropospheric chemistry.

Our previous work with NaCl aerosol particles provided motivation for the current study.⁶ Probe molecule spectroscopy of NaCl aerosol particle surfaces using the solvatochromic probe coumarin 314 (C314) revealed that the surfaces are highly polar, a fact attributable to preferential adsorption of the C314 molecules to defect sites on the surface. While polar solvents produce strong bathochromic shifts, or “red shifts”, in the spectrum of C314, the adsorption of a few molecular layers of water caused a blue shift in both the electronic absorption spectrum and in the ionization threshold of C314 compared with the dry surface. We attributed this counterintuitive result to the rearrangement of the underlying NaCl lattice upon the adsorption of water, changing the interaction of C314 with the surface. The well-known mobility^{7–9} of ions on wet halide surfaces leads to a smoothing of the surface and a reduction in ion–dipole forces experienced by the probe molecule. These results showed the importance of defect sites on aerosol particle surfaces, and highlighted some of the competing effects of local and continuum interactions in determining the overall polarity of the surface.

One way to extend the description of these surfaces is to quantify separately the dipolarity/polarizability contribution to polarity from the hydrogen-bonding character of the surface. In the NaCl example, in addition to the strongly dipolar character of the salt, surface-adsorbed water could hydrogen bond to C314, producing some contribution to the overall solvatochromic shift. Because that work was based on only a single probe molecule, it could only assess the cumulative effect of the surface. Here, we use a multiple probe analysis to better describe surfaces where hydrogen bonding may be an important element. In particular, cases where the surface can act as a hydrogen bond donor (HBD) are of particular interest.

The linear solvation energy (LSE) approach of Kamlet, Abboud, and Taft (KAT) provides a means of performing such an analysis. In their model,^{3,5} the energy of a characteristic transition is described in terms of several model parameters according to the equation

* Corresponding author. E-mail: ewoods@mail.colgate.edu.

$$\tilde{\nu} = \tilde{\nu}_0 + s \cdot \pi^* + a \cdot \alpha + b \cdot \beta \quad (1)$$

In this simplified version of the Kamlet-Taft LSE relationship, $\tilde{\nu}$ is the energy of the spectral feature of interest such as the energy of maximum absorption in an electronic spectrum ($\tilde{\nu}_{\max}$), and $\tilde{\nu}_0$ is a reference value for that absorption in a completely nonpolar medium. The parameters π^* , α , and β represent the solvent's dipolarity/polarizability, hydrogen bond acidity, and hydrogen bond basicity respectively, while the parameters s , a , and b , are solute-specific correlation coefficients that gauge the sensitivity of the solute to each of these solvent characteristics.

This work is the first to apply LSE relationships to aerosol surfaces; however, recent work shows that quantitative polarity measurements are applicable to bulk, flat surfaces as well as powders. For example, Donaldson and co-workers¹⁰ measure the laser-induced fluorescence spectrum of pyrene adsorbed to hexanoic acid coated water surfaces, and the intensity ratio of particular features in the spectrum provides an indicator of polarity.¹¹ Eisenthal and co-workers generated an interfacial polarity scale based on $E_T(30)$ values measured using second harmonic generation spectroscopy.¹² Of particular relevance to the work presented here, Spange and co-workers characterized many different silica, alumina, and aluminosilica solid acid powders using LSE relationships.¹³ They found that these surfaces have a wide range of dipolarity/polarizability terms ($\pi^* = 0.38$ to 1.04) and very large HBD terms ($\alpha = 1.00$ –1.99). Further, they concluded that solid acids display “solvent-like” behavior and are generally well-described by LSE relationships despite some sample-to-sample fluctuations. Spange and co-workers have also determined LSE relationships for functionalized silica particles¹⁴ and cellulose.¹⁵

The present experiment uses a series of four coumarin laser dyes (C153, C314T, C314, C337) as probe molecules, because they have several attributes that complement our experiment. First, their ionization potentials are low (6.8–7.1 eV),^{16,17} which is advantageous to our ionization detection method. Also, the $S_1 \leftarrow S_0$ transition for these compounds is strongly solvatochromic. Last, they are of limited solubility in water and partition to the surface of aqueous solutions, which is advantageous in the preparation of the test aerosols.

This work extends our previous work with NaCl to include $(\text{NH}_4)_2\text{SO}_4$, an important model cloud condensation nucleus,^{18,19} as well as several other test particles that we use to understand trends. Our goal is not only to catalog the relevant parameters for these aerosol surfaces, but to identify the structural and chemical features that determine polarity.

II. Experimental Section

We measure excited-state absorption spectra for molecules adsorbed to aerosol particle surfaces using a two-step, photoionization procedure. This approach is based on previous experiments designed to monitor particulate polycyclic aromatic hydrocarbons (PAH).^{20–23} Our experiment differs mainly in that we use tunable lasers instead of UV lamps as a source of ionizing radiation, enabling the two-step ionization. Breaking the ionization into two steps, excited-state excitation then ionization, enables the measurement of the excited-state spectrum of trace amount of adsorbed molecules.

Aerosol Generation. In most cases, we produce aerosol particles from an aqueous, 295 K source solution (~ 3 g/L salt, $\sim 1 \times 10^{-6}$ M probe) made using distilled, deionized water. Figure 1 shows a schematic illustration of the experiment. An atomizer (TSI model 3075) produces a 2.0 standard liter-per-minute (slpm) flow of air containing aqueous droplets from the

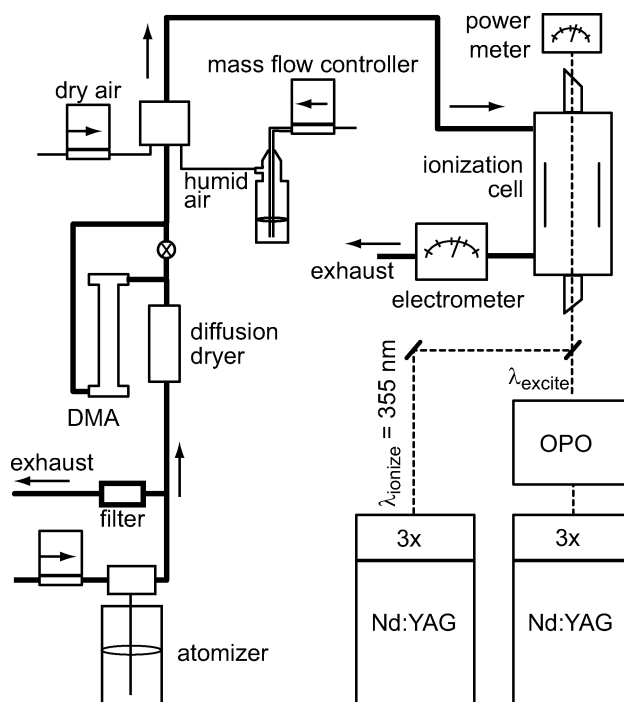


Figure 1. Schematic diagram of the experimental apparatus. The arrows indicate the direction of flow.

source solution. For Al_2O_3 and CaCO_3 , which are insoluble in water, we generate particles by atomizing a suspension of the particles in water. These particles (Duke Scientific) are poly-disperse (300–2000 nm diameter), and some larger particles settle out of suspension. We allow the suspension to rest for 30 min prior to collecting data to ensure that the size distribution and number density remain relatively constant.

Flow System. The first stage of the flow system divides the aerosol stream in a 4:1 ratio, with the larger flow exiting the system through an exhaust. Splitting the flow makes drying the particles easier and avoids photoelectron recombination processes that occur at large particle number densities.²⁴ The smaller, 0.40 slpm flow passes through a diffusion dryer to remove the water solvent, crystallizing the aqueous particles. The resulting solid particles have approximately 50 probe molecules on their surface. This level of coverage effectively excludes interactions between probe molecules. The mean final particle mobility diameter is near 100 nm, and the geometric standard deviation is approximately 1.8. Because the coumarin probe molecules have limited solubility in electrolyte solution, they locate preferentially on the surface of the particle as the nascent droplets dry out and shrink. When the particles reach the effluence RH, the crystals form with coumarin molecules adsorbed to the surface. The dried particle flow passes through a Po-210 static control ionizer (NRD), bringing them into charge equilibrium.

A differential mobility analyzer (DMA) size selects a portion of this flow, which greatly reduces the number density of particles but likewise reduces the spread in probe molecule coverages. Because the number of probe molecules per particle grows as the third power of the radius and the surface area only as the radius squared, the relative surface coverage of probe molecule grows linearly with the particle radius for a given atomizer solution. Size selection also eliminates the possibility of spurious signals arising from the extreme ends of the particle size distribution, where the particle morphology may be different from those whose size is near the mode. The DMA size selects particles near the mean diameter of 100 nm for these experi-

ments. The sheath flow is 4.00 slpm, creating a 10:1 sheath to aerosol flow ratio. The atomizer produces a much lower number density of particles from suspension than it does from homogeneous salt solutions; therefore, we bypass the DMA for the Al_2O_3 and CaCO_3 experiments. In those cases, we use a particle size selector (TSI model 376060) positioned just before the electrometer to ensure that particles smaller than 30 nm make no contribution to the signal.

The next stage of the flow system dilutes the monodisperse aerosol flow to 3.0 slpm using a mixture of dry air and air that is bubbled through water. Controlling the relative amount of dry and humid air tunes the RH, which we monitor using a traceable hygrometer. The measured RH is generally within 5% of the value calculated on the basis of flows, but fluctuates by as much as 3% during a given experiment. The RH-adjusted particles then flow through a 1-liter tank, giving the particles approximately 20 s to reach equilibrium with the water vapor in the flow.

Ionization Scheme. The RH-adjusted aerosol flow interacts with laser light in an ionization cell. A tunable visible photon prepares the excited electronic state and a second, fixed-frequency photon ionizes only the electronically excited molecules. The nascent photoelectrons precipitate out in a small (5 V/cm) electric field. The field is too small to alter the particle trajectories or significantly perturb the spectroscopy. A frequency tripled, 10 Hz Nd:YAG (Spectra Physics) pumps an OPO (OPOtek) to generate the visible light (420 – 510 nm) for the electronic excitation. The line width of the visible radiation is approximately 20 cm^{-1} , and we typically use pulse energies in the range of 1–2 mJ/pulse. A second, frequency-tripled Nd:YAG produces the 355 nm ionization beam. The lasers pass through the cell unfocused, with a beam diameter of 3 mm. Following the ionization of the probe molecules, the aerosols carry a net positive charge. Scanning the visible laser's wavelength while monitoring the charge in the aerosol stream using an aerosol electrometer (TSI model 3068A) produces a signal that reflects the absorption spectrum of the excited state.

Data Collection. For each data point in a scan, the data collection software (LabView) averages the electrometer signal for 3 s (30 laser shots) first with the two lasers synchronized, then again with the ionization laser firing 100 μs after the excitation laser. The first set of data has contributions from the desired visible + UV stepwise ionization, and also from background signals attributable to multiphoton ionization by either the excitation or ionization lasers separately. The second set contains only contribution from the background signals, because the excited-state lifetime is much less than 100 μs . Subtracting these two signals, then, yields the signal resulting only from the desired, stepwise ionization. A 5-second pause in data collection between changing either the laser's timing or wavelength and signal averaging ensures that the particles ionized under the new conditions have enough time to reach the electrometer before signal averaging begins.

III. Results and Analysis

Kamlet-Taft Parameters for Probe Molecules. To generate KAT parameters for aerosol surfaces, one must first characterize the solvatochromic molecules to be used as probes. We use a series of four coumarin laser dyes (C314, C314T, C153, and C337) as probe molecules in our experiment, and Figure 2 shows their structures. Of these molecules, only C153 has previously reported KAT parameters.^{25–27} In general, one determines these parameters by measuring the transition energy of maximum absorption ($\tilde{\nu}_{\text{max}}$) in the UV–vis spectrum for a number of

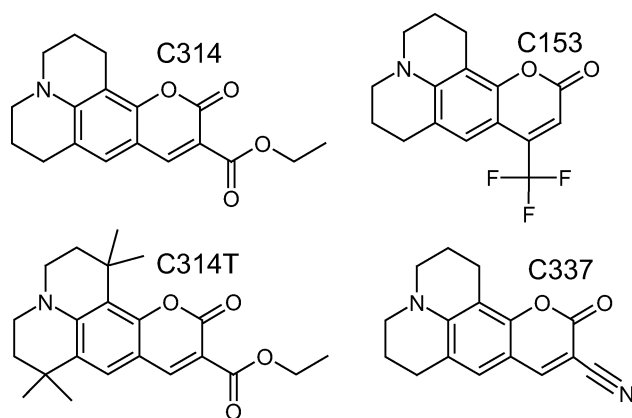


Figure 2. Chemical structures of the four coumarin-derivative probe molecules used in the experiment.

TABLE 1: KAT Parameters for Coumarin Probe Molecules^a

probe	ν_0 (cm^{-1})	S (cm^{-1})	A (cm^{-1})	sd (cm^{-1})	F
C153	25420 (70) ^b	−2080 (120)	−770 (110)	85 ^c	193
C314T	23900 (40)	−860 (70)	−520 (60)	80	173
C314	23900 (50)	−1070 (70)	−490 (60)	79	209
C337	23420 (50)	−1020 (80)	−380 (60)	85	157

^a Solvents: hexane, cyclohexane, benzene, diethyl ether, ethyl acetate, carbon tetrachloride, toluene, tetrahydrofuran, N,N-dimethylformamide, dimethylsulfoxide, acetone, acetonitrile, methanol, ethanol, and butanol. ^b The numbers in parentheses represent the standard error in the fitted parameter. ^c The “sd” values are the standard error in the predicted transition energy, $\tilde{\nu}$.

different solvents whose parameters (π^* , α , β) are well-known. We determine the $\tilde{\nu}_{\text{max}}$ by fitting the spectra to an arbitrary functional form that fits the data well. Fitting the resulting $\tilde{\nu}_{\text{max}}$ values to eq 1 using a step-forward,²⁷ multiple linear regression approach produces the solute parameters s , a , and b . In this step-forward approach, the F statistic serves as a guide to determine which parameters produce statistically significant improvements in the fits.

Table 1 lists the results of the multiple least-square analyses using 15 different organic solvents, including the standard error (sd) and the F statistic. The solvent correlation coefficients, π^* , α and β , are taken from References 4 and 5. For C314, we find that $s = -1090 (\pm 70)\text{ cm}^{-1}$ and $a = -470 (\pm 50)\text{ cm}^{-1}$. Including the $b\beta$ term in the fits does not improve the F statistic and we conclude that it is unnecessary for this molecule. These results are not surprising as C314 has several sites that can accept hydrogen bonds, but none that can donate them. We expect that the two ester sites are the principle hydrogen-bonding sites because of the associated resonance stabilization. The s parameter is similar in the remaining coumarins with the exception of C153, which is markedly more solvatochromic than the others ($s = -2080\text{ cm}^{-1}$). The a parameter varies from -380 cm^{-1} in C337 to -770 cm^{-1} in C153. C314 and C314T have similar structures and correspondingly similar a values, both near 500 cm^{-1} . Only C314T produces a better F statistic by including b in the fits. The resulting b value is small ($\sim 200\text{ cm}^{-1}$), and the improvement in the F statistic is minor ($< 10\%$); therefore, we use the two-parameter description for all probes in our analysis of the model aerosols.

Our values for C153 differ from those reported previously.^{25–27} Our spectroscopic data agree well with those of Molotsky and Huppert,²⁶ but they report a three-parameter description instead of just two, accounting for the discrepancy. Rather than using $\tilde{\nu}_{\text{max}}$, Moog and co-workers²⁷ define the transition energy as the midpoint between the energies where the absorbance is half of

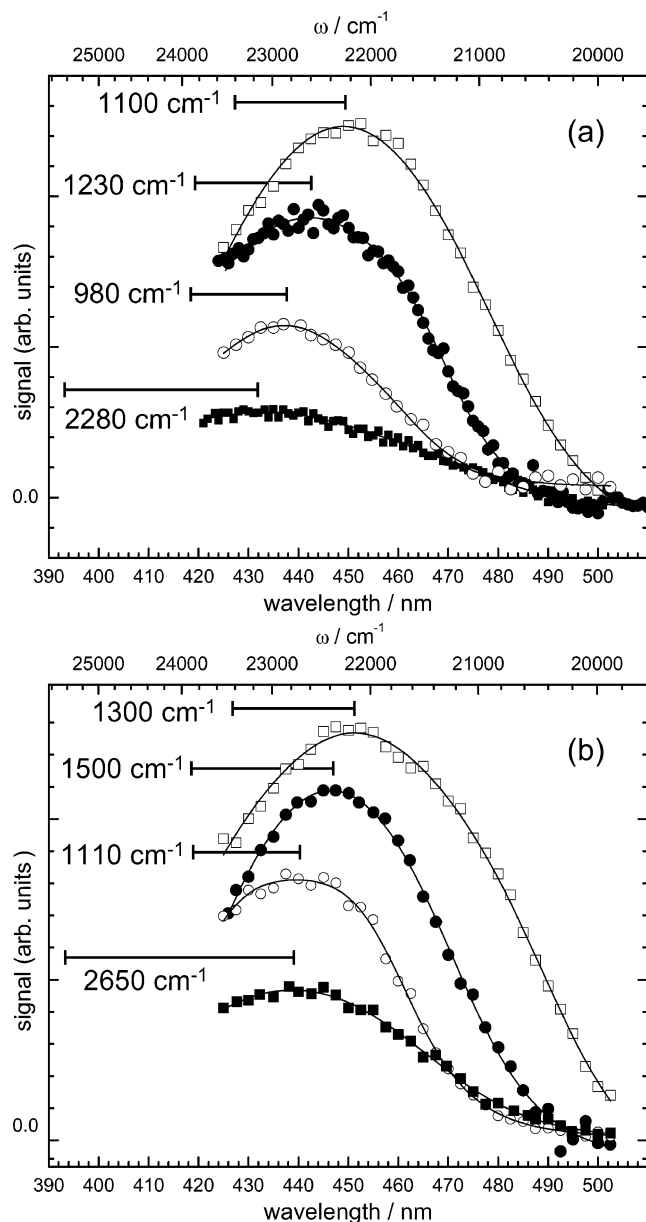


Figure 3. Aerosol photoionization spectra for each of the four probe molecules adsorbed to the surface of (a) $(\text{NH}_4)_2\text{SO}_4$ and (b) NaCl aerosol particles. The combs in the figure connect the fitted maxima in the spectra to the corresponding values for a completely nonpolar medium ($\tilde{\nu}_0$). They represent the total solvatochromic shift for each of the probes. (■, C153; ○, C314T; ●, C314; □, C337).

the maximum value. Because the bands are asymmetric, their LSE parameters are different than ours. We determine $\tilde{\nu}_{\text{max}}$ using the same peak fitting approach for both these UV-vis data as for the aerosol photoionization spectra in the next section. The peak fitting approach works well for cases where one cannot measure the entire spectral envelop, which is the case for our aerosol photoionization spectra (see Figure 3). For consistency, then, we use our KAT parameters for C153 in the analysis that follows.

Aerosol Photoionization Spectra. Figure 3 shows aerosol photoionization spectra for all four coumarin probes adsorbed to a) NaCl aerosol particles and b) $(\text{NH}_4)_2\text{SO}_4$. The combs on the figure connect the value of $\tilde{\nu}_{\text{max}}$ for a particular dye to the corresponding reference value ($\tilde{\nu}_0$) and illustrate the total solvatochromic shift. Table 2 lists the total shifts for each dye adsorbed to several different aerosol surfaces; each shift represents an average of between 3 and 7 independent measure-

ments. In all cases, the solvatochromic shift is very large, a result of the strong ion-dipole interaction with the ionic substrate. Nevertheless, the difference between the largest and smallest solvatochromic shift for C314 in particular is 570 cm^{-1} , which is a similar difference to that between ethanol and cyclohexane. Clearly, these aerosol surfaces present a wide range of electronic environments to adsorbed molecules.

A multiple linear regression of the solvatochromic shifts using the regression parameters s , a , and $\tilde{\nu}_0$ determined for the coumarin probes produces the "solvent" parameters π^* and α . This analysis is essentially the reverse of the one that produces the probe parameters from well-characterized solvent parameters. Table 2 shows the results of this analysis for all of the aerosol surfaces and includes the standard error in the fits (sd) and the F statistic.

A larger and more diverse set of probe molecule structures and, thus, KAT parameters, would be naturally advantageous in generating the aerosol surface parameters. Two separate issues relating to this limitation arise. The first issue is the number of statistically significant parameters, and the second is the uncertainty in the fitted parameters. As with the determination of the probe molecule parameters, the F statistic determines whether a two-parameter description (ie π^* and α vs π^* only) is necessary. For the aerosol parameters, F is larger by at least 30% in all cases where we report both π^* and α rather than just π^* . We estimate the uncertainty in the KAT parameters for the aerosol surfaces by modeling the sensitivity of the fitted parameters using the known uncertainties in both the measured transition energies, $\tilde{\nu}_{\text{max}}$, and the probe molecule parameters, s and a . The greater uncertainty in the α values are attributable to the smaller and more tightly clustered values of the probe molecule a coefficients.

Our previous work on NaCl aerosol particles using only C314 showed that the surface morphology plays an important role in determining the polarity of the surface.⁶ Dry surfaces are rough and molecules adsorbed to defect sites experience large electric fields. For dry NaCl aerosol surfaces in this study, using only the $s\pi^*$ term produces the largest F statistic. This result is consistent with our intuition, as there is only sparse water on the surface and no other possible H-bond donors. The π^* value of 1.29 is higher than that for most homogeneous solvents ($\pi^* = 0-1$),⁵ and such a large value is, again, indicative of the strong ion-dipole interactions. The π^* values are also higher than those for ionic liquids, which are usually near 1.0,^{28,29} again suggesting that the topographical features of the surface play an important role.

The majority of the aerosols behave similarly when the surfaces are dry (<5% RH). For all except two materials, $(\text{NH}_4)_2\text{SO}_4$ and NH_4Cl , the π^* term is the only statistically important one, and the value is at least 1.29. Clearly, these two exceptions are capable of donating H-bonds at low RH, unlike the other salts, all of which are aprotic. A discussion of their lower values of π^* follows in the next paragraph. Excluding the ammonium salts, then, some intuitively appealing trends emerge from the data. From the graphical comparison of π^* values in Figure 4, it is clear that (1) for materials with all singly charged ions, π^* increases with increasing size of the anion ($\text{KI} > \text{NaBr} > \text{NaCl}$), and (2) surfaces with multiply charged ions produces a larger solvatochromic shift than the singly charged species. Statement 1 is a reflection of the polarizability dependence of π^* . On average, the more polarizable surfaces respond to the electronic excitation more strongly. Additionally, the larger anions create a greater lattice parameter, and this increase in charge separation may also contribute to a larger

TABLE 2: KAT Parameters for Aerosol Surfaces

aerosol	% RH	$\tilde{\nu} - \tilde{\nu}_0$ (cm ⁻¹)				π^*	α	sd/cm ⁻¹	<i>F</i>
		C153	C314T	C314	C337				
NaCl	<5	-2590	-1110	-1510	-1390	1.29 (0.05) ^a		60 ^b	370
	65%	-2490	-1140	-1380	-1250	1.00 (0.05)	0.55 (0.15)	20	3210
(NH ₄) ₂ SO ₄	<5	-2170	-1090	-1230	-1050	1.01 (0.05)	0.23 (0.15)	20	1710
	75%	-2540	-1290	-1380	-1350	1.00 (0.05)	0.79 (0.15)	60	170
Na ₂ SO ₄	<5	-2590	-1160	-1410	-1430	1.29 (0.05)		90	150
NH ₄ Cl	<5	-2280	-1180	-1280	-1150	0.73 (0.05)	1.06 (0.10)	10	3130
NaBr	<5	-2850	-1340	-1480	-1490	1.40 (0.05)		100	150
KI	<5	-2850	-1340	-1730	-1390	1.43 (0.10)		140	70
NaNO ₃	<5	-2900	-1340	-1530	-1250	1.39 (0.09)		130	100
CaCO ₃	<5	—	-1440	-1780	-1590	1.62 ^c (0.06)		60	20
Al ₂ O ₃	<5	—	-1450	-1800	-1730	1.69 ^c (0.06)		40	30

^a The numbers in parentheses represent estimates of the uncertainty in the fitted parameter. ^b The “sd” values are the standard error in the predicted transition energy, $\tilde{\nu}$. ^c The data do not permit a clear decoupling of π^* and α in these cases.

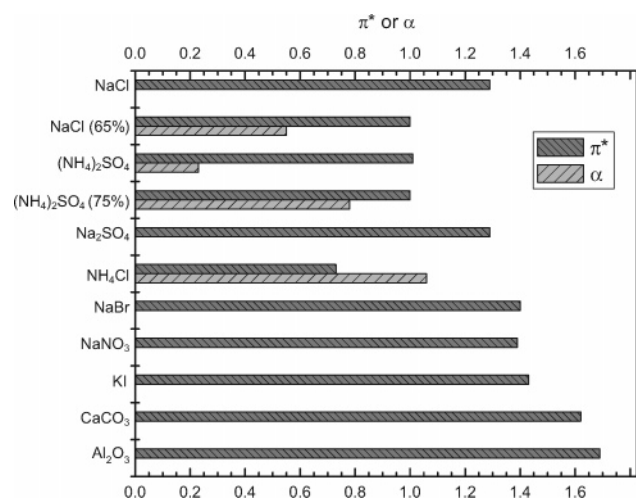


Figure 4. Graphical comparison of the π^* and α values determined from our analysis. Though all would be considered very polar when compared to homogeneous molecular solvents, the data show that these surfaces pose a large range of electronic environments to adsorbed species. A negative correlation between π^* and α is also implied.

π^* . Statement 2 arises strictly from discrete ion-dipole interactions between the probe and surface. Because the local electric field contributes greatly to the overall solvatochromic shift,⁶ the increase in charge causes dramatic shifts in the interaction energy.

Given these two trends, the results for ammonium sulfate are surprising. The sulfate anion is double charged and polarizable, thus one would expect the ammonium sulfate surface to have a π^* value more similar to that of KI or CaCO₃. Furthermore, Table 2 shows that the α parameter makes an appreciable contribution in the linear regression. Because each of the coumarin probes used here has a negative value for the a parameter, the addition of hydrogen-bond donor ability to the surface should increase the solvatochromic shift rather than decreasing it. The other hydrogen-bond donating surface, NH₄-Cl, shows similar behavior. The α value is large (1.06), and its π^* value of 0.73 is the lowest of all the surfaces measured.

While for homogeneous solvents π^* and α are not generally correlated, these results suggest a negative correlation for the surfaces studied here.

We note that both the CaCO₃ and Al₂O₃ surfaces are likely hydroxylated under our experimental conditions, having been aerosolized from an aqueous suspension. We have not been able to measure reproducibly the spectrum of C153 adsorbed to these two substrates. This deficiency, coupled with a larger uncertainty in the other $\tilde{\nu}_{\max}$ values, makes discriminating a one vs two-parameter description difficult. The reported value of π^* , then, reflects only a simple linear regression with the $s\pi^*$ term.

We offer two explanations for the apparent negative correlation between α and π^* . The first is that strong hydrogen-bonding interactions may orient the coumarin probe molecules such that the continuum, or nonspecific, interaction with the surface weakens. For example, the coumarin probes may bond with the molecular plane tilted away from the surface rather than lying flat, as Figure 5 depicts. In this case, the largely delocalized frontier orbitals¹⁶ of the probes are exposed to air more so than in the flat geometry, causing a decrease in π^* . Alternatively, strong local interactions on defect-free surfaces may compete with adsorption to defect sites, effectively reducing the exposure of the probe to these highly polar sites. In either case, the observation that strong local interactions between the probe and surface can cause an overall decrease in the surface polarity may be quite general and illustrative of the important differences between surfaces and homogeneous solvents.

While there is relatively little LSE data for surfaces in the literature, the characterization of aluminosilicates by Spange and co-workers¹³ supports our simple picture of a negative correlation between π^* and α for surfaces. Although they attribute the observation to the changing Al:Si ratio in the powders that they studied, we suggest that either of our possible explanations may also contribute to the observation.

Applying this approach to NaCl and (NH₄)₂SO₄ aerosols at elevated RH reveals the effect of adsorbed water on the chemical environment of the probe molecule. For NaCl, π^* is chemically constant up to approximately 60% RH, where $\pi^* = 1.25$, a slightly lower value than at low RH. The decrease in π^* is

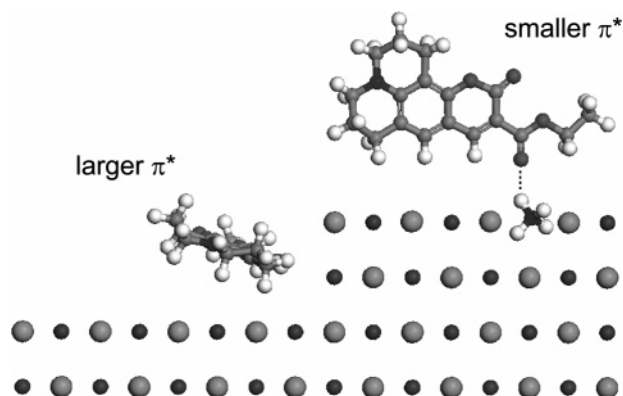


Figure 5. A model scenario to explain the observation that hydrogen-bonding surfaces have lower π^* values. The left side of the figure shows C314 adsorbed near a defect site on the surface. This geometry leads to large ion-dipole forces. The right-hand side shows a C314 molecule hydrogen bonded to an ammonium ion on the surface. In this case, the molecule interacts less strongly with the surface ions.

consistent with a slight smoothing of the surface facilitated by adsorbed water, as observed before.⁶ At 65% RH, very close to the deliquescence RH of 75%, the fits show an increase in the α parameter to 0.55 and a further decrease in π^* to 1.00. Because of the steep dependence of the adsorbed water layer thickness on RH near the deliquescence point³⁰ and our limited control over the RH, it is necessary to consider these KAT parameters as an average over a range of water coverages on the order of several molecular layers. Nevertheless, these data indicate the onset of direct solvation of the coumarin probe molecules by the adsorbed water.

In contrast to NaCl, $(\text{NH}_4)_2\text{SO}_4$ surfaces become more polar at higher RH with an increasing contribution from the HBD term ($\pi^* = 1.00$ and $\alpha = 0.79$). We conclude that the direct solvation of probe molecules by water is relatively more important on $(\text{NH}_4)_2\text{SO}_4$ surfaces than on NaCl surfaces. This difference between NaCl and $(\text{NH}_4)_2\text{SO}_4$ is another illustration that the bonding geometry of the probe molecule to the surface controls the polarity. In our picture of the strongly oriented, hydrogen-bonded coumarin, the molecular plane is more accessible to solvation than it would be if it were lying flat. This simple picture qualitatively accounts for the trends in our data.

These results suggest that surfaces may be reliably studied using this approach, as evidenced by the good correlations in our fits. If there were large differences in the way these probes interacted with a particular surface, then one would expect poorer statistics. It is likely that the similar shape and functionality of these coumarin derivatives aids in producing consistent results.

The results also highlight some important differences between surfaces and homogeneous solvents. In particular, one must consider not just the composition of the aerosol surface, but also the topography of the surface and the orientation of the adsorbed molecule. These details are discrete in nature as opposed to the more continuum-like effect that is usually associated with π^* . In applying these results to the organic components of tropospheric aerosol, one should recognize how the shape, size, and functionality of the adsorbed molecules all facilitate interaction with defect sites or hydrogen-bonding sites. These discrete characteristics are as important as continuum interactions in determining the overall polarity.

IV. Conclusion

Linear solvation energy parameters are effective in describing aerosol particle surfaces and demonstrate some important factors

in determining the polarity of surfaces. As expected, these ionic surfaces are highly polar as a result of discrete ion-dipole interactions. Furthermore, polarizable species and multiply charged ions lead to increases in polarity, as measured by the π^* parameter. The particle morphology and the nature of the bonding of the probe molecule with the surface produce results that are somewhat counterintuitive compared to homogeneous solvents. In particular, strong hydrogen bond interactions produce an overall drop in polarity by altering the bonding geometry with the surface. Likewise, adsorbed water can either produce a decrease or increase in overall polarity depending on the surface.

Acknowledgment. EWIII acknowledges support from the American Chemical Society Petroleum Research Fund (44099-GB6).

References and Notes

- Reichardt, C. *Chem. Rev.* **1994**, *94*, 2319.
- Spange, S.; Lauterbach, M.; Gyra, A. K.; Reichardt, C. *Liebigs Ann. Chem.* **1991**, 323.
- Abboud, J. L.; Kamlet, M. J.; Taft, R. W. *J. Am. Chem. Soc.* **1977**, *99*, 8325.
- Laurence, C.; Nicolet, P.; Dalati, M. T.; Abboud, J.-L. M.; Notario, R. *J. Phys. Chem.* **1994**, *98*, 5807.
- Kamlet, M. J.; Abboud, J. L. M.; Abraham, M. H.; Taft, R. W. *J. Org. Chem.* **1983**, *48*, 2877.
- Woods, E.; Morris, S. F.; Wivagg, C. N.; Healy, L. E. *J. Phys. Chem. A* **2005**, *109*, 10702.
- Dai, Q.; Hu, J.; Salmeron, M. *J. Phys. Chem. B* **1997**, *101*, 1994.
- Luna, M.; Rieutord, F.; Melman, N. A.; Dai, Q.; Salmeron, M. *J. Phys. Chem. A* **1998**, *102*, 6793.
- Ghosal, S.; Shbeeb, A.; Hemminger, J. C. *Geophys. Res. Lett.* **2000**, *27*, 1879.
- Mmerek, B. T.; Donaldson, D. J. *J. Phys. Chem. Chem. Phys.* **2002**, *4*, 4186.
- Kalyanasundaram, K.; Thomas, J. K. *J. Am. Chem. Soc.* **1977**, *99*, 2039.
- Wang, H.; Borguet, E.; Eisenthal, K. B. *J. Phys. Chem. B* **1998**, *102*, 4927.
- Spange, S.; Vilsmeier, E.; Zimmermann, Y. *J. Phys. Chem. B* **2000**, *104*, 6417.
- Prause, S.; Spange, S.; Barthel, H. *Macromol. Chem. Phys.* **2005**, *206*, 364.
- Spange, S.; Fischer, K.; Prause, S.; Heinze, T. *Cellulose* **2003**, *10*, 201.
- Kovac, B.; Novak, I. *Spectrochim. Acta, Part A* **2002**, *58*, 1483.
- Novak, I.; Kovac, B. *J. Electron Spectrosc. Relat. Phenom.* **2000**, *113*, 9.
- Abbatt, J. P. D.; Broekhuizen, K.; Kumal, P. P. *Atmos. Environ.* **2005**, *39*, 4767.
- Broekhuizen, K.; Chang, R. Y. W.; Leitch, W. R.; Li, S. M.; Abbatt, J. P. D. *Atmos. Chem. Phys.* **2006**, *6*, 2513.
- Niessner, R. *J. Aerosol Sci.* **1986**, *17*, 705.
- Niessner, R.; Wilcox, C. F. *Anal. Chem.* **1989**, *61*, 708.
- Hueglin, C.; Paul, J.; Scherrer, L.; Siegmann, K. *J. Phys. Chem. B* **1997**, *101*, 9335.
- Kasper, M.; Keller, A.; Siegmann, K.; Siegmann, H. C. *J. Electron Spectrosc. Relat. Phenom.* **1999**, *98–99*, 83.
- Mohr, M.; Burtscher, H. *J. Aerosol Sci.* **1997**, *28*, 613.
- Fischer, K.; Prause, S.; Spange, S.; Cichos, F.; Von, Borczykowski, C. *J. Polym. Sci., Part B* **2003**, *41*, 1210.
- Molotsky, T.; Huppert, D. *J. Phys. Chem. A* **2003**, *107*, 8449.
- Moog, R. S.; Kim, D. D.; Oberle, J. J.; Ostrowski, S. G. *J. Phys. Chem. A* **2004**, *108*, 9294.
- Crowhurst, L.; Falcone, R.; Lancaster, N. L.; Llopis-Mestre, V.; Welton, T. *J. Org. Chem.* **2006**, *71*, 8847.
- Crowhurst, L.; Mawdsley, P. R.; Perez-Arlandis, J. M.; Salter, P. A.; Welton, T. *J. Phys. Chem. Chem. Phys.* **2003**, *5*, 2790.
- Foster, M. C.; Ewing, G. E. *J. Chem. Phys.* **2000**, *112*, 6817.